Received: 11 July 2022 | Revised: 17 August 2022 | Accepted: 20 August 2022

DOI: 10.1002/app.53124

RESEARCH ARTICLE

Applied Polymer SCIENCE WILEY

Enhanced miscibility of PBAT/PLA/lignin upon γ-irradiation and effects on the non-isothermal crystallization

Janetty Jany Pereira Barros[1,2] | **Carlos Pereira Soares**[2] | **Esperidiana Augusta Barretos de Moura**[2] | **Renate Maria Ramos Wellen**[1,3]

[1]Academic Unit of Materials Engineering, Federal University of Campina Grande, Campina Grande, Brazil

[2]Centro de Química e Meio Ambiente, Instituto de Pesquisas Energéticas e Nucleares, São Paulo, Brazil

[3]Materials Engineering Department, Federal University of Paraíba, João Pessoa, Brazil

Correspondence
Janetty Jany Pereira Barros, Academic Unit of Materials Engineering, Federal University of Campina Grande, Campina Grande 58249-140, Brazil.
Email: jany.barros@certbio.ufcg.edu.br

Funding information
Fundação de Apoio à Pesquisa do Estado da Paraíba, Grant/Award Number: 017/2019; Conselho Nacional de Desenvolvimento Científico e Tecnológico, Grant/Award Number: 303426/2021-7; Coordenação de Aperfeiçoamento de Pessoal de Nível Superior, Grant/Award Number: 88887.569630/2020-00; IAEA-CRP, Grant/Award Number: 17760/RO; Fundação de Apoio à Pesquisa do Estado de São Paulo, Grant/Award Number: 2019/00862-9

Abstract

Lignin is natural and renewable polymer, the second most abundant on Earth. Properly used it can reduce synthetic and oil based materials in addition to contributing to the biodegradable systems. In this work, the kraft lignin was subjected to gamma radiation at absorbed doses of 30, 60, and 90 KGy in order to increase the interaction with "Poly(butylene adipate-co-terephthalate) (PBAT)/Poly(lactic acid) (PLA)" blend (Ecovio®). PBAT/PLA/lignin blends with 10% of the weight of lignin were produced by extrusion using twin-screw extruder and characterized by Fourier transform infrared spectroscopy (FTIR), Differential scanning calorimetry (DSC), and Field emission scanning electron microscopy (FE-SEM). FTIR spectra showed partial miscibility between PBAT/PLA and lignin, most due to the hydrogen bond between PBAT/PLA carbonyl and lignin hydroxyl, being intensified in irradiated lignin compounds. As evidenced on DSC scans, in PBAT/PLA/irradiated lignin the crystallization peak was shifted to lower temperatures and the crystallization rate decreased. Crystallization kinetics was modeled using Pseudo Avrami, and isoconversional models of Friedman and Vyazovkin. Pseudo-Avrami displayed linearity deviation at beginning and crystallization ending due to the nucleation and secondary crystallization, while from Friedman and Vyazovkin the activation energy (*Ea*) was higher for PBAT/PLA/irradiated lignin 30 KGy, characterizing crystallization with higher energy consumption. FE-SEM images showed better dispersion and miscibility in PBAT/PLA/irradiated lignin. The results indicate that the irradiation of Kraft lignin promotes miscibility and compatibility of PBAT/PLA/lignin.

KEYWORDS

biopolymers and renewable polymers, crystallization, differential scanning calorimetry (DSC), irradiation, kinetics

1 | INTRODUCTION

Lignin is a natural polymer that attracts great attention due to the renewable character as well as to be the second most abundant on Earth, just behind cellulose which is the first one. Lignin has an aromatic structure, where the monomeric repeating units form a three-dimensional network.[1,2] The lignin available on the

market is produced mainly by bioethanol and by the paper industry, where it is treated as by-product originated from the cellulose extraction.[1,3] Lignin is highly functional; it has phenolic and aliphatic hydroxyl groups that can be widely exploited/reacted or modified. The presence of these different groups makes lignin an excellent component to produce materials based on ecologically polymers and confer properties such as stabilizing effect, reinforcing, absorption of ultraviolet rays (UV), biodegradability, and antimicrobial activity.[3,4]

Despite its wide availability, the industrial application of lignin is quite limited,[3,4] its use does not correspond to its potential; most of the industrial lignin is used as a low-cost fuel for energy generation. Another characteristic that makes its use difficult it is its complex and reticulated structure; therefore, physical and chemical modifications are used to expand the application of lignin.[4,5]

Ionizing radiation is a promising tool to control polymer properties and an alternative route to functionalize lignin expanding its use in thermoplastic applications. Irradiation of polymers such as gamma rays, leads to the excited states formation, that is, reactive intermediate products such as ions and free radicals, several reaction pathways that result in rearrangement and/or formation of new bonds and structures.[6–9] Researches have shown benefits of ionizing radiation to improve polymeric composites properties with lignocellulosic fibers, such as adhesion improvement between fiber and matrix, heading to better mechanical properties, improvement in water resistance, and thermal stability.[10,11]

Poly(lactic acid) (PLA) is a linear aliphatic polyester produced from renewable sources, mainly starch and sugar.[12] PLA had good optical, physical, and mechanical properties compared to petroleum-based polymers.[13] However, PLA has disadvantages that drawbacks its application, such as low impact strength and poor barrier properties. Blending is an alternative to solve this problem. Poly(butylene adipate-co-terephthalate) (PBAT) becomes an excellent possibility to improve the ductility and processability of PLA, as it is a flexible and biodegradable aliphatic-aromatic copolyester.[14,15] The PLA/PBAT/Lignin blend has great potential for applications in mulching films.

Kumar et al.[16] used gamma radiation to compatibilize bio-based PLA/lignin. It was observed that PLA and irradiated lignin at absorbed dose of 30 KGy are compatible, unlike blends with non-irradiated lignin. PLA/irradiated lignin blends with the crosslinking agent, triallyl isocyanurate, showed significant improvement in mechanical and thermal properties and slow hydrolytic degradation compared to PLA with non-irradiated lignin. Irradiated lignin displayed continuous phase morphology without any significant phase separation. El-Zayat, et al.[11] reported irradiated lignin-filled polyvinyl alcohol/gelatin mixtures for antimicrobial packaging materials, it was verified that irradiation promoted improvements in the materials' thermal stability.

Chen et al.[17] investigated biobased PLA/PBAT/lignin blends, through Fourier transform infrared spectroscopy (FTIR) analysis, it was verified that lignin-polyester interaction involves hydrogen bonds. Other researches have already been reported on PLA/PBAT systems.[18,19] However, due to the structural difference between PBAT/PLA, these blends tend to result in poor properties, limiting their applications. Ecovio® can be an interesting alternative to this obstacle, since it is PBAT/PLA blend, consolidated in the market with advantages such as biodegradability and flexibility which are excellent for applications as films and disposables.

During semicrystalline polymers processing, crystallization and melting are the most important phase transitions. To understand crystallization, it is necessary to elucidate the crystallization kinetics and consider the degree of crystallinity with time and temperature, as well as the crystallization relationship with thermophysical properties.[20,21] Polymer processing usually takes place under dynamic conditions, so understanding non-isothermal crystallization is of great relevance. Models that describe the crystallization kinetics are fundamental guides in polymer processing. From them, the materials behavior can be reliably predicted. Isoconversional methods have advantages over the conventional ones, as they provide precise kinetic information about the involved processes, in addition to providing important parameters, such as the relationship between the degree of crystallinity with time and temperature, activation energy, crystallization rate, enabling the evaluation between theoretical and experimental deviations which are indicative of the applied models predictive power.[22,23]

Literature has reported the crystallization kinetics of PLA/PBAT with a third constituent, such as PLA/PBAT/silver loaded kaolinite[24]; PLA/PBAT/titanate-treated calcium carbonate[25]; PLA/PBAT/Talc.[26] However, from our knowledge, there is lack on the PBAT/PLA/Lignin and its crystallization kinetics which it can be of great importance since lignin addition to PBAT/PLA may provide potential biodegradable materials with bactericidal, antioxidant, UV barrier properties and better mechanical properties, hence, deep understanding of the crystallization kinetics can be used as proper tools for the rational control to reach the best relationship among processing, structure and properties. [3,4,14,15]

The objective of this work was to produce biodegradable blends based on non-irradiated and irradiated Lignin (30, 60, and 90 KGy radiation doses) added to PBAT/PLA blend. Afterwards, analyzing the effect of gamma radiation on PBAT/PLA/lignin, chemical and thermal properties as well as the non-isothermal crystallization kinetics using Pseudo-Avrami, Friedman, and Vyazovkin modeling.

2 | METHODOLOGY

2.1 | Materials

PBAT/PLA blend (82% PBAT and 18% PLA) the commercial grade Ecovio® F2332 from BASF SE (Ludwigshafen, Germany) with the following properties: melt flow index equal 7.0–11.0 g/10 min (2.16 kg at 190°C), density 1.24–1.26 g/cm^3, melting point equal to 140–155°C, and water vapor permeation rate (23°C, 50% r. h.) equal to 120 cm^3/(m^2·d·bar). Lignin Kraft obtained from agro-industry residues, such as eucalyptus, supplied by Suzano (São Paulo, Brazil), (pH: 3.8; solids content: 95%; ash content: 2%).

2.2 | Lignin washing

Kraft lignin was previously washed to remove residual impurities. A solution of 200 ml of 0.01 mol/L HCL was added to 20 g of lignin, following the solution was submitted to magnetic stirring during 30 min, afterwards, the suspension was filtered using vacuum pump (Quimis-Brasil), after filtering the lignin was washed with deionized water until reaching 6 < pH <7 aiming to reduce the lignina acidity. After washing, the lignin was sent for drying in an oven with air circulation at 60 ± 2°C for 48 h. Then the lignin was macerated and sieved in a #200 mesh.

2.3 | γ-irradiation

The sieved lignin was submitted to gamma radiation at 5.0 KGy/h at room temperature, to obtain irradiated lignin at absorbed doses of 30, 60, and 90 KGy, using the Cobalt-60 Multipurpose Gamma Irradiator of the Technology Center of IPEN, São Paulo.

2.4 | Materials processing

PBAT/PLA and lignin were initially dried in an air circulating oven at 80°C for 24 hours, to remove moisture before processing. PBAT/PLA blend with 10wt% of lignin were melt blended using a corotating twin-screw extruder Haake Rheomex with 16 mm and L/D = 25 from Thermo Scientific. The extruder temperature profile was 145/155/160/155/140/140°C, and the screws rotation were 6 rpms. The extruded coming out of the extruder were cooled down in the air for better dimensional stability, pelletized by a pelletizer, dried in an air circulating oven at 80°C for 24 h, and the specimens for characterization were kept in a plastic bag.

2.5 | Characterizations

2.5.1 | Chemical analysis using Fourier transform infrared spectroscopy (FTIR)

FTIR analyses were performed using the Perkin Elmer – Frontier. Tests carried out in the medium infrared range with wavenumber ranging from 4000 to 650 cm^{-1}, with 16 scans and resolution of 4 cm^{-1} with the attenuated total reflectance accessory.

2.5.2 | Field emission scanning electron microscopy (FE-SEM)

PBAT/PLA/Lignin samples were cryofractured under liquid nitrogen and their surfaces' morphology were analysed by scanning electron microscopy (FE-SEM) using the Thermo Fisher Scientific equipment, model Quanta FEG 650. Prior to SEM analysis, samples were covered with Platinum (Pt) in the Baltec equipment, model MED-020.

2.5.3 | Differential scanning calorimetry (DSC)

DSC analyses were carried out using a Mettler Toledo DSC 822. Samples with approximately 4–5 mg were sealed in aluminum crucibles; the purge gas used was nitrogen with a gas flow of 20 ml/min. A three-stage thermal cycle was applied: samples were heated from −30 to 200°C, remaining at 200°C for 3 min (isotherm), after which the melt was cooled to −30°C (cooling) and reheated to 200°C, it was done in order to analyse the existence of crystallization and melting events. Tests were performed under non-isothermal conditions, at constant heating/cooling rates: 5; 10; 15; and 20°C/min. Kinetic modeling was performed using Netzsch's Kinetics Neo Software, and a custom software was employed to obtain the relative crystallinity and the crystallization rate as function of time and temperature, methodology elsewhere reported (Arruda et al.[27]).

2.5.4 | Theoretical background – crystallization kinetics

The kinetics of reactions in solids is generally described by Equation (1):

$$\frac{d\alpha}{dt} = k(T)f(\alpha) \quad (1)$$

Where $f(\alpha)$ is the reaction model, α is the reaction extent, $k(T)$ is the Arrhenius rate constant, T is the temperature, t is the time. For non-isothermal environment, when temperature changes with time at constant rate, $\Phi = \frac{dT}{dt}$.[28]

Equation (1) is applied to a single reaction mechanism process. The global transformation process may involve multiple mechanisms characterized by different $k(T)$ and $f(\alpha)$. The constant rate $k(T)$ and the reaction model $f(\alpha)$ must be specified correctly to accurately determine the reaction rate. Arrhenius equation often describes the constant rate, Equation (2)[29]:

$$k(T) = A.e^{-\frac{Ea}{RT}} \tag{2}$$

Where A is the pre-exponential factor, Ea is the effective activation energy of the reaction mechanism, and R is the universal gas constant.

The polymer crystallization process is mainly studied through kinetic analysis. However, misuse of a model or rate constant in experimental data can lead to physically meaningless or misleading results. Macroscopic kinetics is complex, as it includes information about several steps that occur simultaneously, requiring effective methods to obtain reliable results, such as isoconversional methods. The fundamental assumption of isoconversional methods is that the single-step Equation (1) is applicable only to a single conversion extension and the temperature region ΔT related to that conversion. In other words, isoconversional methods describe the kinetics of the process using several single-step kinetic equations, each of which is associated to a defined extent of conversion. Based on this assumption, isoconversional methods allow complex (i.e., multi-step) processes to be detected through Ea variation with Ref. [30].

2.5.5 | Pseudo-Avrami modeling

Traditional Avrami model[31,32] is often used to analyse isothermal crystallization processes. Avrami's model correlates the relative degree of crystallinity X as a function of time t measured from the beginning of the event according to Equation (3):

$$X = 1 - \exp(-Kt^n) \tag{3}$$

Where K is the rate constant related with nucleation and crystal growth rates and n is the Avrami exponent that depends on the nucleation nature and crystal growth geometry. The non-isothermal crystallization data obtained at constant cooling rates can be correlated by an expression analogous to Avrami's Equation (4)[33,34]:

$$y = \ln\left(\ln\frac{1}{1-x}\right) = \ln K' - n'\ln\tau \tag{4}$$

Where τ is the time since the onset of the non-isothermal crystallization event, measured at a constant heating/cooling rate.

However, the model parameters K' and n' are functions of the cooling/heating rate Φ, not the temperature, as in the Avrami model, this empirical correlation model is called Pseudo-Avrami, which transfers the mathematical precept from the Avrami equation for the non-isothermal kinetic data, thus circumventing Avrami's original requirement of isothermal crystallization conditions.[34,35]

2.5.6 | Friedman isoconversional modeling

Friedman's differential isoconversional method[36] determines Ea without assuming the reaction type, using points with the same conversion from measurements with different heating rates or different isothermal conditions. Apparent Ea is calculated for various degrees of conversion according to Equation (5):

$$\ln\left(\frac{d\alpha}{dt}\right) = lnA + lnf(\alpha) - \frac{Ea}{RT} \tag{5}$$

Where t is time, T is temperature, α is the extent of conversion from amorphous (liquid or solid) to crystalline phase, A is the pre-exponential factor, Ea is the activation energy, and $f(\alpha)$ is the reaction model related to the mechanism. From Equation (5), if the function $f(\alpha)$ is constant for a particular value of α then the sum $lnA + lnf(\alpha)$ is also constant.[37,38]

2.5.7 | Vyazovkin isoconversional modeling

Vyazovkin[28] developed a nonlinear integral isoconversional method, just for a set of several dynamic measurements. This method is based on the fact that Ea is independent of the heating rate and, therefore, for experiments performed at "n" heating rates, the ratio of the temperature integral in each conversion extension remains constant. Mathematically it can be written as, Equation (6):

$$\sum_{i=1}^{n}\sum_{j\neq i}^{n} I[E_{A\alpha_i}, T_{\alpha_i}]\beta_j / \left(I\left[E_{A\alpha_j}, T_{\alpha_j}\right]\beta_i\right) = n(n-1) \tag{6}$$

As the temperature values of the experimental data can have some errors, the strict equality of the above

equation can be approximated to the absolute function minimum, that is, the value closest to zero, Equation (7):

$$\left|\sum_{i=1}^{n}\sum_{j\neq i}^{n} I[E_{A\alpha_i}, T_{\alpha_i}]\beta_j / \left(I\left[E_{A\alpha_j}, T_{\alpha_j}\right]\beta_i\right) - n(n-1)\right| = min \tag{7}$$

Where the indices i and j denote the set of experiments performed under different heating rates, n is the total number of experiments.

3 | RESULTS AND DISCUSSION

3.1 | Fourier transform infrared spectroscopy (FTIR) measurements

Figure 1 shows FTIR spectra of non-irradiated and irradiated lignin at absorbed doses of 30, 60, and 90 KGy. The identified bands at 3395 cm^{-1} are attributed to —OH vibration, at 2939 and 2840 cm^{-1} they are attributed to C—H elongation in aliphatic portions, at 1602 cm^{-1} is attributed to C═C group of the ring, conjugated structures. Upon irradiation, the intensity of the absorption band at 1602 cm^{-1} increased and it was higher for higher radiation doses, that is, 60 and 90 KGy, indicating an increase in lignin conjugation during irradiation and suggesting that cleavage of phenoxy groups due the irradiation led to formation of conjugated groups in lignin.[39] The bands 1514, 1453, and 1411 cm^{-1} are attributed to C—H deformation vibration, absorption bands at 1266 and 1136 cm^{-1} are stretching vibrations of Guaiacyl and Siringil's carbonyl group units, respectively, at 1211 cm^{-1} OH deformation of phenolic hydroxyl group, at 1105 cm^{-1} C—O stretching vibration.[40,41]

Upon irradiation, there was increase in the absorption intensity bands and displacement of hydroxyl group band, 3395 cm^{-1}, to lower wavelength, 3275 cm^{-1}, which can be attributed to the fact that γ-irradiation induced the breakdown of some functional groups and promoted increase of OH groups whereas some of them with higher bonds energy, that is, were shifted to lower wavenumber. Increase of C═O and C═C on lignin is also reported.[40,41] When lignin is irradiated with γ rays, the absorbed radiation energy by lignin alters the molecular electronic energy resulting in valence electron transitions causing various physical and chemical processes.[9,42]

During lignin irradiation process, the OH groups dissociation occurs, so variations in the FTIR spectrum and degradation occur through C—O—C bond cleavage, producing primary radicals, which are trapped in the lignin matrix even at room temperature, as the glass transition temperature (Tg) of lignin is around 130°C. Some of the primary free radicals undergo secondary processes such as dehydration and water elimination leading to the formation of double bonds or poly-conjugated structures, observed in the band increase at 1602 cm^{-1}.[9,42]

From the OH band integration using Fytik software,[43] the corresponding band area was evaluated as presented in Figure 2, hence, it is clear that increasing the radiation dose, the amount of OH groups increased, suggesting lignin chain scission, Figure 2. Additionally, the band peak has displaced to lower wavenumber indicative of higher energy OH bonds.

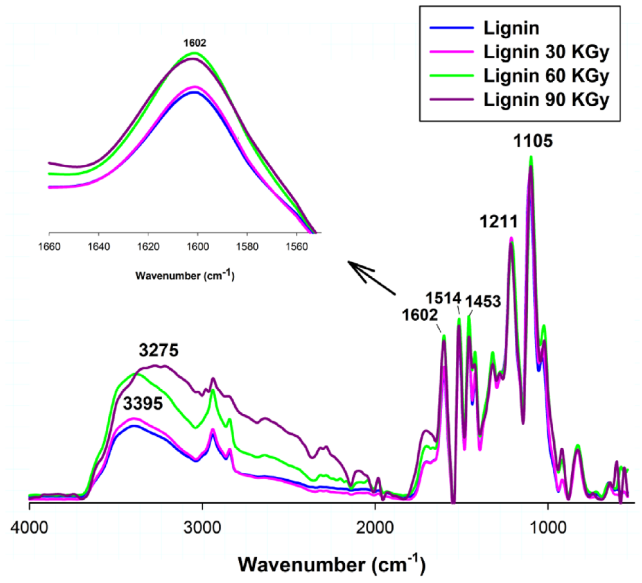

FIGURE 1 Fourier transform infrared spectroscopy spectra of non-irradiated lignin and irradiated lignin at doses of 30, 60, and 90 KGy. [Color figure can be viewed at wileyonlinelibrary.com]

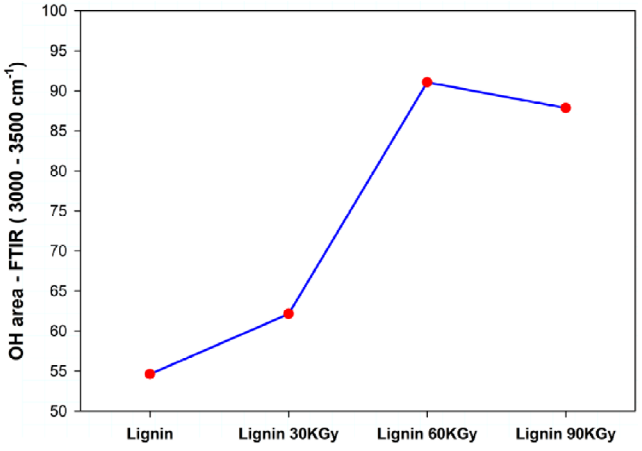

FIGURE 2 Value of the corresponding area of OH band in the Fourier transform infrared spectroscopy wavenumber: 3000–3500 cm^{-1}. [Color figure can be viewed at wileyonlinelibrary.com]

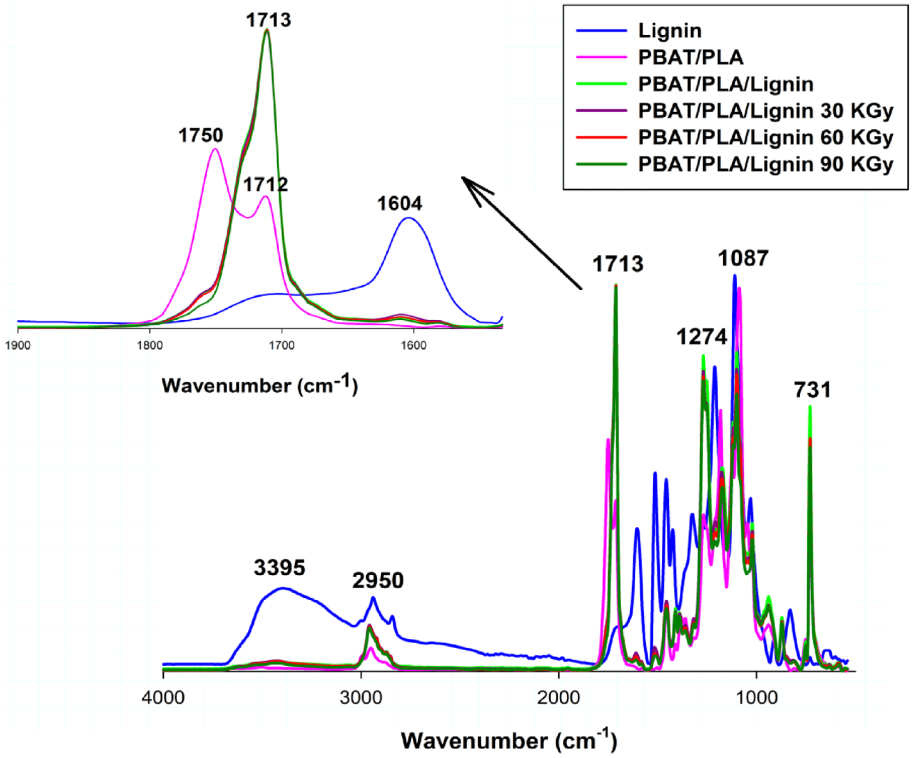

FIGURE 3 Fourier transform infrared spectroscopy spectra of PBAT/PLA, lignin, and PBAT/PLA/lignin at different gamma radiation doses. PBAT, Poly(butylene adipate-co-terephthalate); PLA, Poly(lactic acid) [Color figure can be viewed at wileyonlinelibrary.com]

Figure 3 illustrates FTIR spectra of PBAT/PLA, lignin, PBAT/PLA/lignin and PBAT/PLA/lignin irradiated at doses of 30, 60, and 90 KGy.

PLA and PBAT have different carbonyl bands due to differences in neighboring chemical structures. PLA has carbonyl stretch at 1750 cm^{-1} while PBAT has carbonyl stretch at 1712 cm^{-1}. Upon lignin addition, there were significant changes in this band, shift to intermediate wavelength, increase in absorption intensity and overlap. This suggests that there is strong interaction between PBAT/PLA and lignin provided by secondary bonds such as hydrogen bonds, and formation of only one peak with higher intensity indicates that lignin improves compatibility between PBAT and PLA.[44]

In addition, the blends' OH bands areas were computed, Table 1, presenting values lower than the corresponding 10wt% of lignin added into PBAT/PLA, suggesting intermolecular interaction between the carbonyls in PBAT/PLA and hydroxyls in lignin, which can be translated as strong indication of miscibility among the blends constituents, that is, PBAT/PLA/lignin.

The band at 1455 cm^{-1} is attributed to the asymmetric and symmetrical elongation of CH_3 bonds in PBAT and PLA.[45,46] The bands at 1087, 1165, and 1268 cm^{-1} indicate symmetrical elongation of C═O bonds (ester and carboxylic acid) and asymmetrical elongation of C—O—C bonds found in PBAT and PLA, these bands also underwent alterations upon lignin addition, confirming the existence of interaction between PBAT/PLA/lignin by secondary hydrogen bonds. The band at 939 cm^{-1} is attributed to the symmetrical elongation of C═O bonds and the out-of-plane elongation attributed to the OH sites. The band at 731 cm^{-1} refers to methylene [—$(CH_2)_4$] and the elongation of C═H bonds found in the aromatic rings of PBAT.[47]

TABLE 1 Value of the area corresponding to the OH band in the Fourier transform infrared spectroscopy wavenumber: 3000–3500 cm^{-1}

Compound	OH band area
Lignin	54.6247
Lignin 30 KGy	62.1382
Lignin 60 KGy	91.0722
Lignin 90 KGy	87.8728
PBAT/PLA	1.0858
PBAT/PLA/lignin	2.9441
PBAT/PLA/lignin 30 KGy	4.2759
PBAT/PLA/lignin 60 KGy	3.8790
PBAT/PLA/lignin 90 KGy	3.0260

Abbreviations: PBAT, Poly(butylene adipate-co-terephthalate); PLA, Poly(lactic acid).

3.2 | Differential scanning calorimetry (DSC) measurements

Figure 4 presents non-isothermal DSC scans for non-irradiated lignin and irradiated lignin at doses of 30, 60,

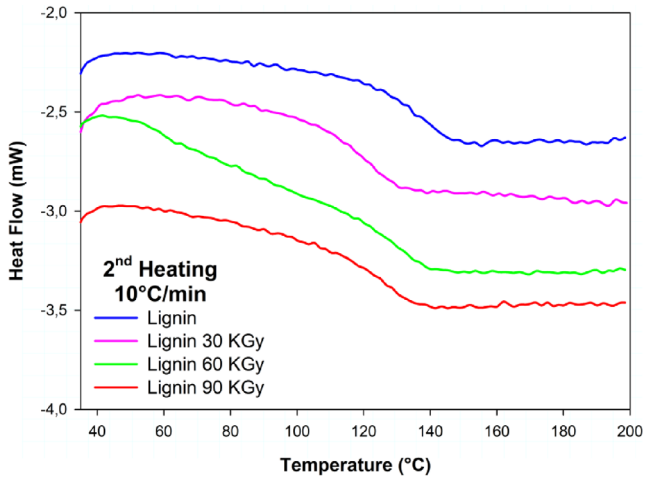

FIGURE 4 Differential scanning calorimetry scans acquired during the second heating. Heating rates and compounds indicated. [Color figure can be viewed at wileyonlinelibrary.com]

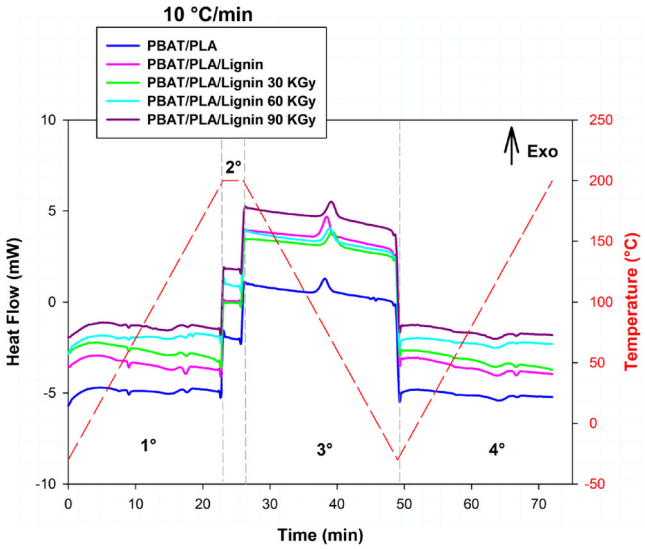

FIGURE 5 Acquired DSC scans for the whole applied thermal program. 1°: Heating stage. 2°: Isotherm. 3°: Cooling stage. 4°: Re-heating stage. [Color figure can be viewed at wileyonlinelibrary.com]

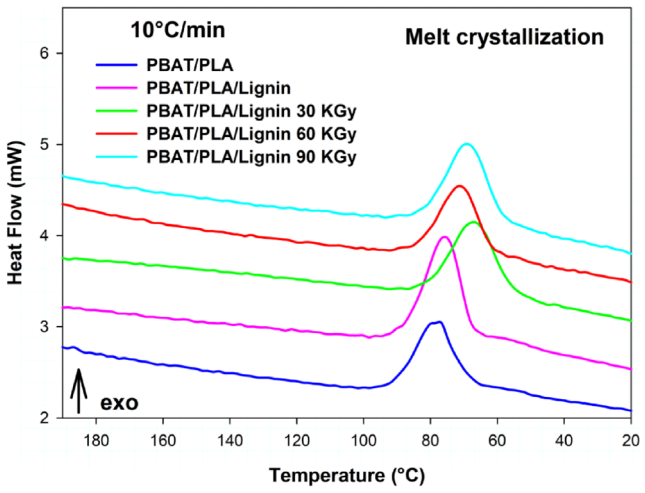

FIGURE 6 Differential scanning calorimetry scans acquired during the cooling. Heating rates and compounds indicated. [Color figure can be viewed at wileyonlinelibrary.com]

and 90 KGy acquired during the second heating. As lignin is an amorphous polymer, melting and crystallization events are not observed, therefore DSC scans are characterized by the glass transition temperature (*Tg*) of lignin, which displayed initial temperature around 125°C. Upon irradiation, *Tg* decreased to 109°C (Lignin 30 KGy), 116°C (Lignin 60 KGy), and 112°C (Lignin 90 KGy). This decrease in *Tg* may be attributed to decrease in the molecular weight resulted from irradiation as well as plasticization phenomena in lignin that arise due to intermolecular action and interaction of hydroxyl groups.[39] Decreased *Tg* of lignin caused by irradiation has already been reported.[39,48]

Figure 5 shows DSC scans acquired during the whole applied thermal program: 1st heating; 2nd isotherm; 3rd cooling; and 4th second heating for PBAT/PLA, PBAT/PLA/lignin and PBAT/PLA/lignin irradiated at absorbed doses of 30, 60, and 90 KGy. In the first heating, all plots presented Tg of PLA, ~60°C and two endothermic peaks associated with the fusion of PBAT and PLA (present in Ecovio®). During cooling, all plots showed an exothermic peak characteristic of PBAT/PLA melt crystallization. For the second heating it can be identified PLA *Tg* ~ 60°C and two subsequent endothermic events, the first one occurs in the temperature range from ~90 to 137°C which is associated to PBAT melting and the second from ~140 to 153°C due to PLA crystals melting.[49]

In Figure 6 it is verified that lignin addition shifted the crystallization peaks to lower temperatures, the most evident effect was viewed in PBAT/PLA/lignin 30 KGy, which decreased ~11.5°C. Thus, lignin addition hindered PBAT/PLA crystallization which required much energy to be developed.

Livi et al.[50] reported that addition of 20% by weight of lignin into PBAT/PLA led to the appearance of a small melting peak at 148°C. Furthermore, added lignin promoted slight increase in *Tg* as well as significant increase in the melting temperature from 117 to 124°C of PBAT. These results might be related with interactions between lignin hydroxyl groups and PBAT $(CH\text{-}COO)_2$.

3.3 | Melt crystallization

Figure 7a,b show the melt crystallization sigmoids acquired from DSC scans integration. It is verified that

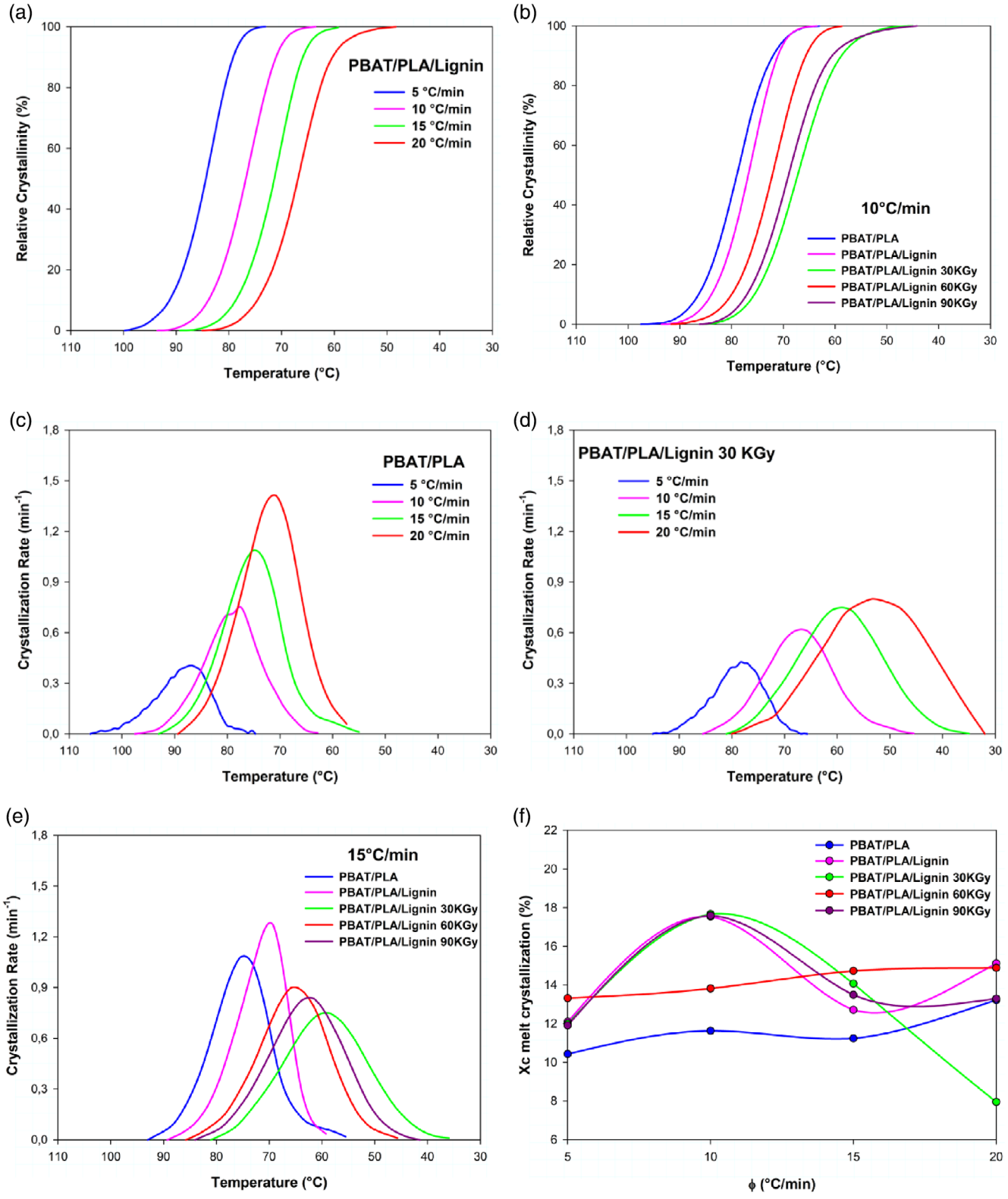

FIGURE 7 Melt crystallization data gathered during cooling. (a) Sigmoids of PBAT/PLA/lignin collected at indicated cooling rates. (b) Sigmoids of PBAT/PLA and PBAT/PLA/lignin collected at 10°C/min. (c) Melt crystallization rates of PBAT/PLA at indicated cooling rates. (d) Melt crystallization rates of PBAT/PLA/lignin at indicated cooling rates. (e) Melt crystallization rates of PBAT/PLA and PBAT/PLA/lignin collected at 15°C/min. (f) Degree of crystallinity of PBAT/PLA and PBAT/PLA/lignin collected during cooling. Compounds indicated. PBAT, Poly(butylene adipate-co-terephthalate); PLA, Poly(lactic acid) [Color figure can be viewed at wileyonlinelibrary.com]

TABLE 2 Crystallization parameters of PBAT/PLA, PBAT/PLA/lignin and PBAT/PLA/lignin irradiated at doses of 30, 60, and 90 KGy

Compound	Φ (°C/min)	5	10	15	20
PBAT/PLA	C_{max} (min^{-1})	0.40	0.77	1.08	1.41
	$T_{0.01}$ (°C)	105.2	95.5	91.6	88.0
	T_P (°C)	88.4	79.0	75.3	71.9
	$T_{0.99}$ (°C)	75.2	63.7	55.7	56.6
	ΔH (J/g)	11.49	12.82	12.37	14.57
	ΔX_c (%)	10.43	11.63	11.23	13.22
PBAT/PLA/lignin	C_{max} (min^{-1})	0.44	0.80	1.28	1.55
	$T_{0.01}$ (°C)	99.2	91.9	87.1	83.6
	T_P (°C)	84.3	76.7	71.3	65.8
	$T_{0.99}$ (°C)	73.9	64.4	58.7	49.0
	ΔH (J/g)	13.32	19.33	14.01	16.66
	ΔX_c (%)	12.09	17.54	12.71	15.12
PBAT/PLA/lignin 30 KGy	C_{max} (min^{-1})	0.43	0,62	0.74	0.87
	$T_{0.01}$ (°C)	93.1	84.3	79.2	77.6
	T_P (°C)	78.7	67.2	59.4	54.0
	$T_{0.99}$ (°C)	67.8	47.1	36.8	36.4
	ΔH (J/g)	13.2	19.47	15.51	8.77
	ΔX_c (%)	11.99	17.67	14.07	7.95
PBAT/PLA/lignin 60 KGy	C_{max} (min^{-1})	0.41	0.72	0.90	1.01
	$T_{0.01}$ (°C)	96.4	90.3	84.2	80.3
	T_P (°C)	81.4	72.1	65.4	60.1
	$T_{0.99}$ (°C)	66.3	58.7	46.3	37.6
	ΔH (J/g)	14.69	15.23	16.23	16.42
	ΔX_c[5] (%)	13.32	13.8	14.73	14.89
PBAT/PLA/lignin 90 KGy	C_{max} (min^{-1})	0.42	0.64	0.83	1.00
	$T_{0.01}$ [1] (°C)	95.0	85.0	82.4	78.5
	T_P [2] (°C)	80.1	68.9	62.1	57.5
	$T_{0.99}$ [3] (°C)	67.3	44.9	43.8	38.3
	ΔH [4] (J/g)	13.13	19.38	14.87	14.65
	ΔX_c[5] (%)	11.91	17.59	13.49	13.29

Abbreviations: ΔH, latent heat of crystallization; ΔX_c, change in crystallinity during the event; PBAT, Poly(butylene adipate-co-terephthalate); PLA, Poly(lactic acid); $T_{0.01}$, temperature of 0.1% crystallized fraction (a good estimate of the event initial point); $T_{0.99}$, temperature of 99.9% crystallized fraction (a good estimate of the event final point); T_P, peak crystallization temperature.

increasing cooling rate shifted the peaks temperature (*Tp*) to lower values. Faster cooling rates mean shorter residence time at each temperature for the polymer to crystallize, that is, nucleation and growth mechanisms which are observed in lower temperatures. Furthermore, increasing the cooling rate can also promote imperfect and/or irregular crystals.[33]

Regarding the composition effect, lignin addition shifted the peaks to lower temperatures, being more evident in PBAT/PLA/lignin 30 KGy, suggesting that at 30 KGy the lignin interacted more with PBAT/PLA, it is also supposed that at 30 KGy lignin suffered greater chain scission, which also resulted in lower *Tg* (Figure 4). It is suggested that at 30 KGy lignin has more reactive functional groups susceptible to interact easily with PBAT/PLA all together hindered the melt crystallization, that is, more energy is needed for crystallization begging/development.[51] Corroborating with FTIR data, where intermolecular interaction was observed between PBAT/PLA C═O of and lignin OH. Thus, the greater the interaction, the greater the difficulty for the macromolecule chains to crystallize. On the other hand, in most

compounds ΔH_c and ΔX_c increased upon lignin addition, Table 2. The melt crystallization rate and the degree of crystallinity are also illustrated, Figure 7c–f. The crystallization rate increased with addition of non-irradiated lignin and decreased with addition of irradiated lignin, Figure 7a, indicating that irradiated lignin presents more secondary interactions, making crystallization difficult, nevertheless with subtle changes in degree of crystallinity.

Xing et al.[52] observed similar results when analyzing DSC scans of UV-barrier PBAT/lignin films. It was reported that PBAT initial crystallization temperature ($T_{0.01}$) changed from 82 to 74°C, upon addition of 10% by weight of lignin and to 69°C upon addition of 20% by weight of lignin. Indicating that lignin hampered PBAT melt crystallization, probably by restricting the polymer chains movement. However, when the required energy for crystallization is reached, lignin favors crystallization.

3.4 | Non-Isothermal crystallization kinetics evaluated using Pseudo-Avrami modeling

Figure 8 shows Pseudo-Avrami plots for PBAT/PLA and PBAT/PLA/lignin 30 KGy. In general, Pseudo-Avrami model was significantly representative, with low linearity deviations which were only observed at the beginning and at the end of crystallization, corresponding to the nucleation and secondary crystallization stages, more evident at the cooling rate of 5°C/min.

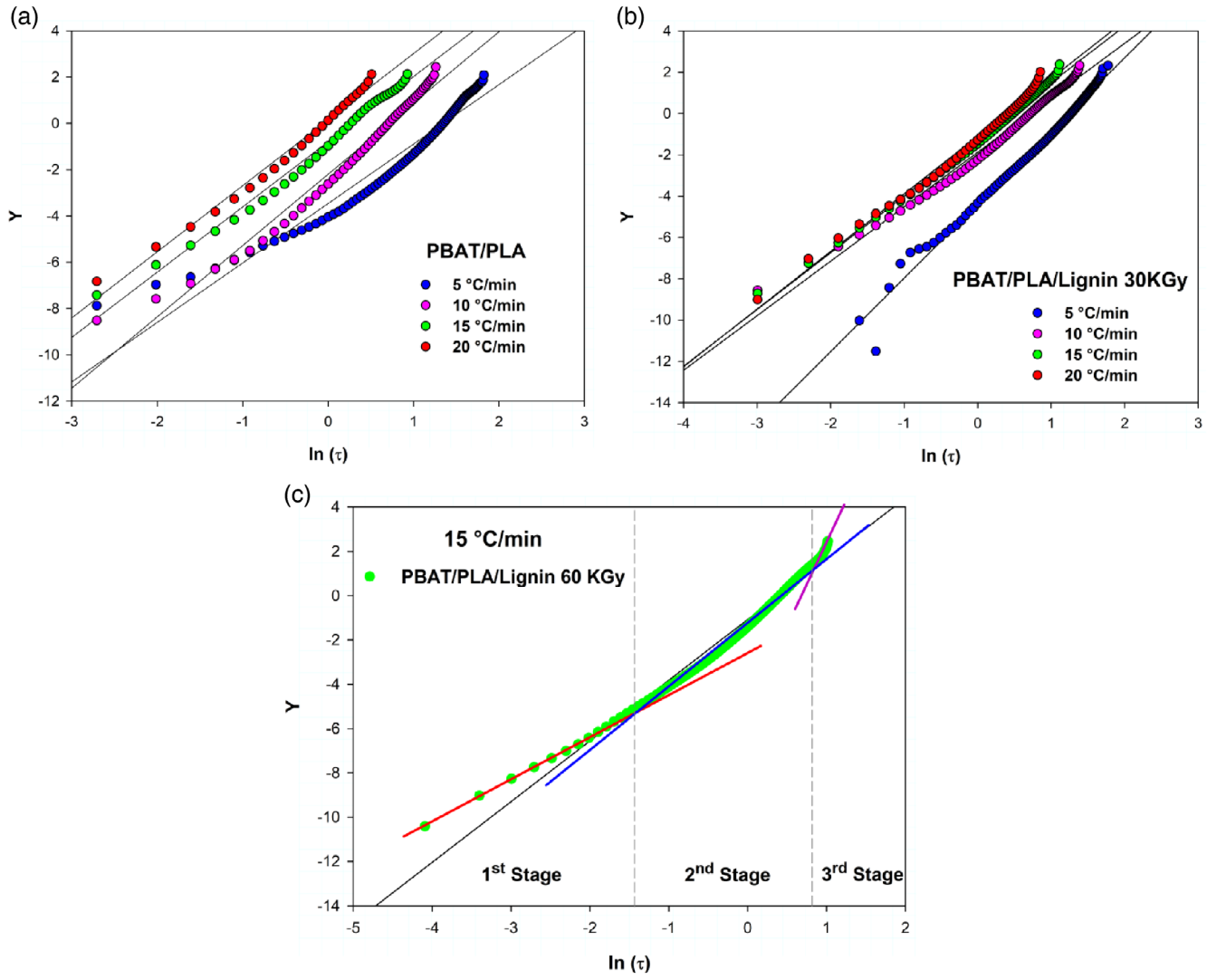

FIGURE 8 Pseudo-Avrami plots (a) PBAT/PLA; (b) e PBAT/PLA/lignin 30 KGy e (c) PBAT/PLA/lignin 60 KGy. Cooling rate of 15°C/min illustrating the crystallization in three stages: 1st nucleation; 2nd primary crystallization; and 3rd secondary crystallization. PBAT, Poly(butylene adipate-co-terephthalate); PLA, Poly(lactic acid) [Color figure can be viewed at wileyonlinelibrary.com]

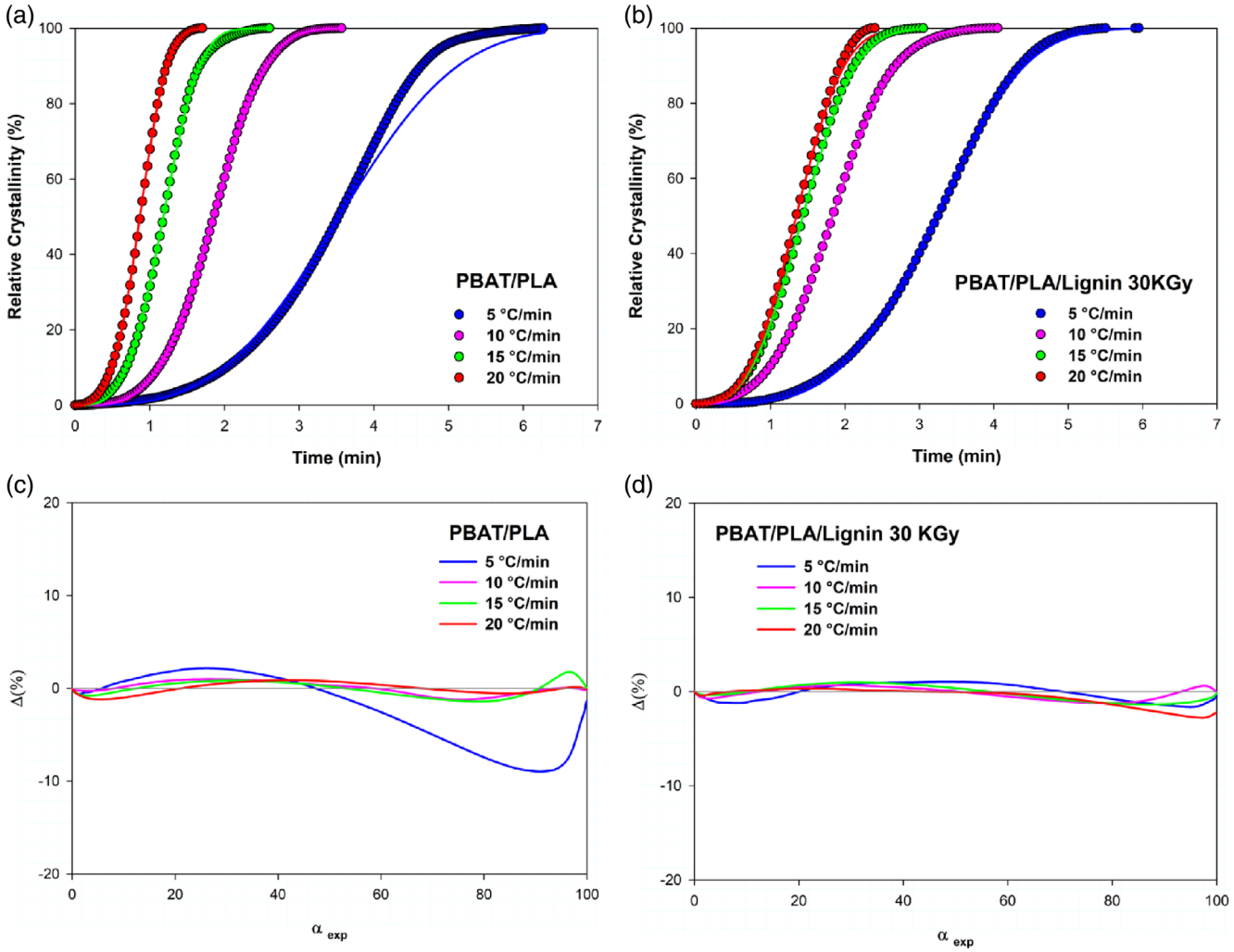

FIGURE 9 (a) and (b) Relative crystallinity of experimental (symbols) and theoretical (solid line) data evaluated using Pseudo-Avrami modeling. (c) and (d) Discrepancy between experimental and theoretical Pseudo Avrami data. Compounds and cooling rate indicated. [Color figure can be viewed at wileyonlinelibrary.com]

In Figure 9a,b, plots of the relative crystallinity as time function are presented. Sigmoidal trend is verified whereas the crystalline stages, that is, three stages are observed:

1. Nucleation: $0\% < X < 10\%$
2. Primary crystallization: $10\% < X < 80\%$
3. Secondary crystallization: $X > 80\%$

An excellent fit between the experimental and theoretical of Pseudo-Avrami data is observed and it can be affirmed that the model was able to satisfactorily predict the melt crystallization of PBAT/PLA and PBAT/PLA/lignin 30 KGy, with subtle deviations as already mentioned at the beginning and crystallization ending. These deviations are possibly due to restrictions on nucleation (whereas more time/energy are required for irradiated lignin) and spherulites growth during secondary crystallization.[53]

Figure 9c,d shows the discrepancy between the theoretical and experimental data for PBAT/PLA and for PBAT/PLA/lignin 30 KGy. In PBAT/PLA, there is deviation between $-9 \leq \Delta X \leq 2$, while for PBAT/PLA/lignin 30 KGy the deviation range is $-2 \leq \Delta X \leq -1$, the highest deviations were obtained for PBAT/PLA/lignin, reaching -14%, compounds with irradiated lignin at 60 and 90 KGy reached maximum deviation of -8% and -2%, respectively, (These data are presented in the Supplementary Information S1) indicating that the model fits better when irradiated lignin is added due to irradiation altering lignin chemical structure, increasing functional groups number, promoting greater intermolecular interaction, and improving miscibility and compatibility, as seen in the FTIR results, Figure 3 and further on in the FEG-MEV results, Figure 15.

Sousa et al.[54] investigated the non-isothermal melt crystallization kinetics of PCL/PBAT, it was reported that

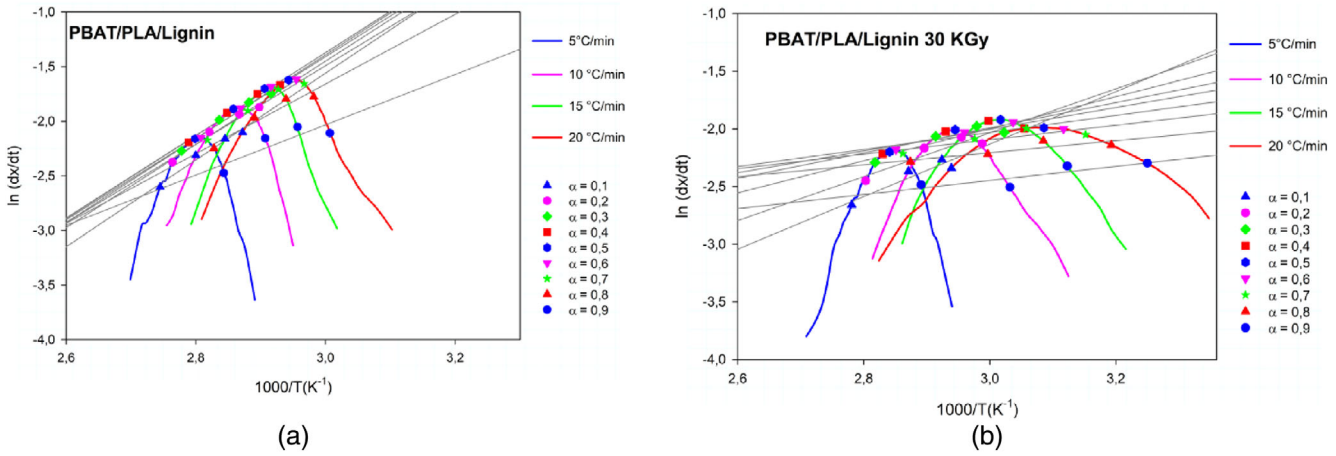

FIGURE 10 Friedman isoconversional linear regression ln (dα/dt) versus 1000/T for PBAT/PLA/lignin and PBAT/PLA/lignin 30 KGy at indicated degrees of conversion. PBAT, Poly(butylene adipate-co-terephthalate); PLA, Poly(lactic acid) [Color figure can be viewed at wileyonlinelibrary.com]

it can be represented by the Pseudo-Avrami model with a reasonable discrepancy, $+8 \leq \Delta X \leq -15$, suitable for processing applications.

Despite the excellent fit obtained using Pseudo-Avrami, it is a macroscopic kinetic model, with limitations, such as not being able to distinguish the details or stages of nucleation and crystalline growth. Microscopic kinetics is responsible for multi-step phenomena that occur simultaneously and requires computational methods. Isoconversion methods, for example, use the data in different temperature programs and evaluate the activation energy as the reaction/process progresses, being able to provide more accurate and meaningful information and parameters.[55]

3.5 | Non-isothermal crystallization kinetics evaluated using Friedman isoconversional modeling

Figure 10 displays the linear regressions acquired using Friedman model for PBAT/PLA/lignin and PBAT/PLA/lignin 30 KGy, from these plots *Ea* was evaluated and acquired data are presented in Figure 11.

Ea dependence with the relative crystallinity is shown in Figure 11. For the melt crystallization process, *Ea* showed negative values, since energy must be removed so that the chain segments are ordered and stuck on the crystalline structure, that is, crystallization advances as the temperature decreases.[33] Namely, *Ea* values are positive when crystallization is initiated by heating (cold crystallization) and negative during melt cooling (crystallization during cooling).[56,57]

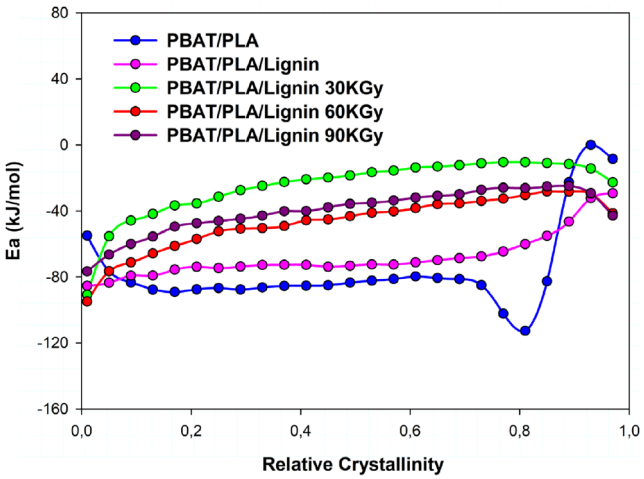

FIGURE 11 *Ea* as relative crystallinity function evaluated using Friedman isoconversional model. Blends indicated. [Color figure can be viewed at wileyonlinelibrary.com]

In general, *Ea* increases with increasing relative crystallinity, indicating that more energy must be supplied for the macromolecules get ordered. For PBAT/PLA in the relative crystallinity range $0.7 \leq \Delta X \leq 1$, can be seen that *Ea* plot changes which is indicative of crystallization mechanism changing.

Vyazovkin and Sbirrazzuoli[57] reported similar result for PET crystallization. It was verified predominantly negative *Ea* values, with a breakpoint at $\alpha = 0.85$ where authors associated it to a change in the crystallization mechanism, that is, from regime I to regime II.

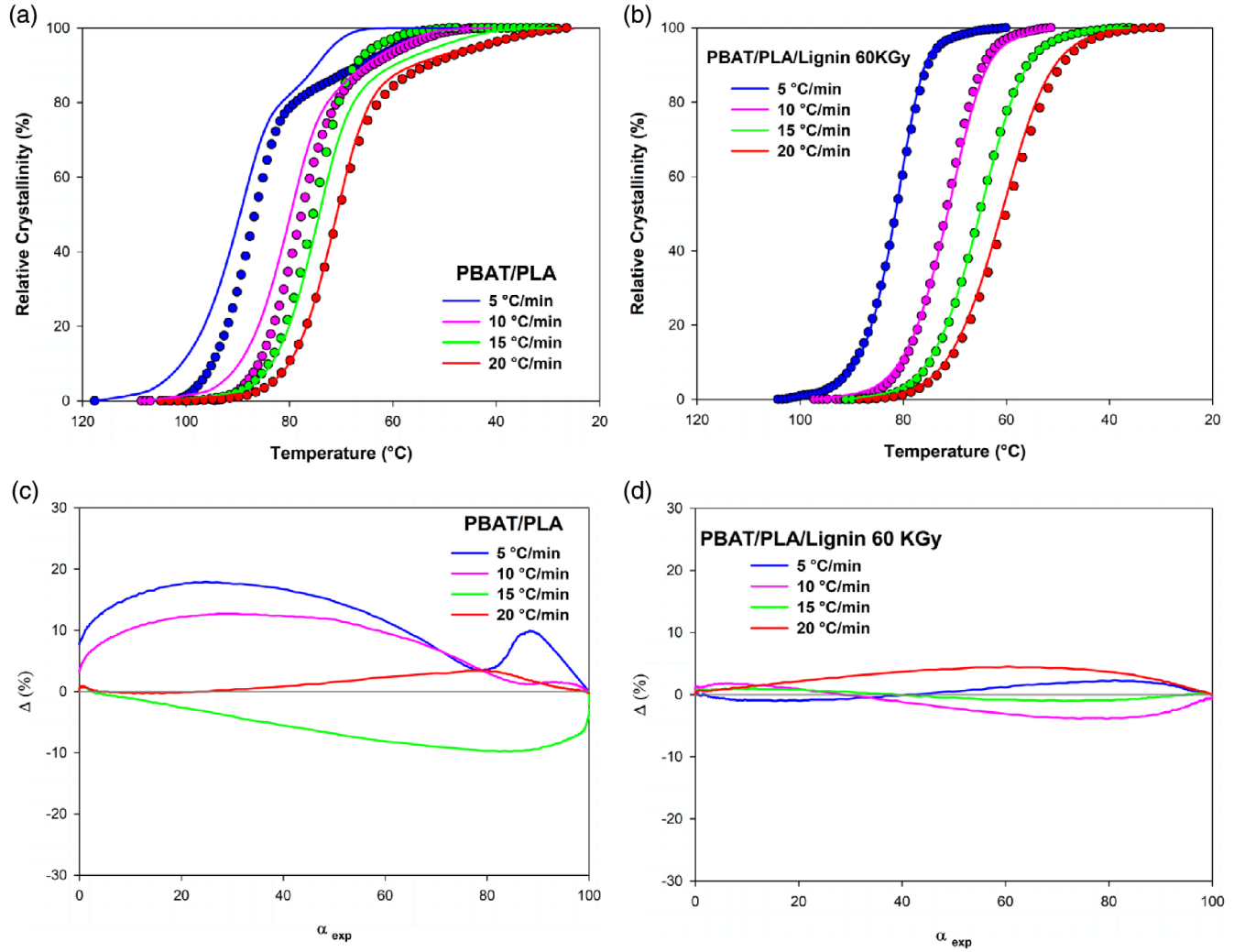

FIGURE 12 (a) and (b) Relative crystallinity as temperature function, experimental (symbols) and theoretical (solid line) data evaluated using Friedman isoconversional model. (c) and (d) Discrepancy between experimental and theoretical data (Δ) using Friedman model at indicated heating rates and blends. [Color figure can be viewed at wileyonlinelibrary.com]

Regime I represent the extreme situation when the single surface core initiates the growth of a crystalline layer. Regime III is the opposite when a new crystalline layer is created through the formation of multiple small nuclei that are so numerous that they practically cannot grow. Regime II comprises an intermediate case in which the layer develops through the several nuclei followed by their growth. In regime I the surface nucleus formation rate is slower than the rate of crystal growth, while in regime II the nucleation rate becomes greater than the growth rate.[56,57]

Regarding the lignin effect, increase in *Ea* is observed, mainly in PBAT/PLA/lignin based on irradiated lignin. Crystallization is controlled by nucleation and diffusion of molecular chains. Lignin addition to PBAT/PLA can act as a nucleating agent and increase X_c, as seen in Figure 7f and Table 2, but at the same time it can hinder molecular movement, delaying crystallization and increasing *Ea*, this trend is more evident upon irradiated lignin addition that have undergone chain scission and have more reactive functional groups susceptible to interact more easily with PBAT/PLA and thus hindering crystallization.[51]

Huang[51] observed similar trend when evaluating *Ea* dependence in PBT/clay nanocomposites using Friedman modeling during non-isothermal crystallization. It was found that at lower X_c, PBT/clay nanocomposites showed lower *Ea* than neat PBT; however, at higher X_c, the nanocomposites exhibited higher *Ea*.

Figure 12a,b illustrate the relative crystallinity as temperature function. For PBAT/PLA, fits between experimental and theoretical data are not satisfactory, with discrepancy between $-10 \leq \Delta X \leq 17$, Figure 12c. This may be linked to the fact that PBAT/PLA is a blend with

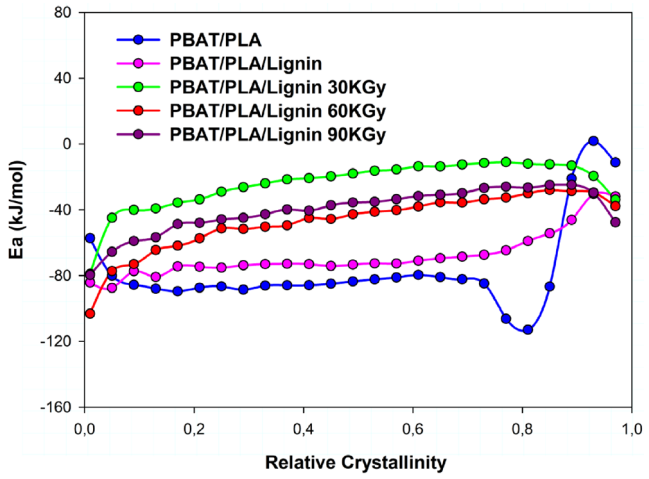

FIGURE 13 *Ea* versus relative crystallinity evaluated using Vyazovkin isoconversional modeling. Blends indicated. [Color figure can be viewed at wileyonlinelibrary.com]

two crystallizable components, PBAT and PLA, and in the DSC scans two melting peaks were visualized, indicating that different crystals may have been developed, in addition to the crystallization mechanism change as presented in *Ea* data of Figure 11.

For PBAT/PLA/lignin compounds with irradiated and non-irradiated lignin, an excellent fit between the data is observed, with discrepancy below 10% and between $-3 \leq \Delta X \leq 5$ for the PBAT/PLA/Lignin 60 KGy, Figure 12b,d. Suggesting that lignin crystallization is governed by only one crystallization mechanism and the Friedman model is significant to determine crystallization kinetics.

3.6 | Non-isothermal crystallization kinetics evaluated using Vyazovkin isoconversional modeling

Figure 13 displays *Ea* trend as relative crystallinity function; plots showed similar behavior to that presented by Friedman modeling, that is, all compounds had negative *Ea*. Upon crystallization progress *Ea* tended to increase as also did upon lignin addition; mainly in the compounds with irradiated lignin. The effect was more evident for PBAT/PLA/lignin 30 KGy. Mechanism changing is also suggested to take place during PBAT/PLA crystallization, similarly to the observed during Friedman modeling.

Acquired results clearly demonstrated a systematic dependence *Ea* with the conversion/relative crystallinity. An increasing dependence of *Ea* on conversion is found mostly for competitive reactions, although some independent and consecutive reactions can also give rise to such dependence.[50,51] As the nonlinear procedure developed by Vyazovkin reveals extremely low errors (<0.1%) in the calculation of activation energy, it can be said that the results are significant.[28]

As PBAT/PLA is a blend with limited interaction between constituents and with different melting temperatures, the higher melting component (PLA) crystallizes in contact of the lower melting component (PBAT). On the other hand, the lower melting PBAT, crystallizes in contact with higher melting PLA. PBAT crystallization occurs heterogeneously (i.e., in contact with solid PLA). Hence, formation of different crystals types is supposed, resulting in heterogeneous morphology, as shown in SEM images, Figure 15

After *Ea* decreasing at $\alpha \geq 0.78$, attributed to the crystallization advance, an increasing profile is observed, which occurs in the conversion interval referring to secondary crystallization, which is probably due to the greater difficulty in ordering the components with lower crystallizability or increasing the perfection of crystallites formed during primary crystallization.

Upon lignin addition, mainly irradiated, there is blend miscibility improvement, through interaction provided by secondary bonds.

Figure 14 displays the fit between the experimental and theoretical data acquired using Vyazovkin modeling. It is observed that PBAT/PLA results were not satisfactory, not showing a good fit between plots and reaching a maximum discrepancy of −25%, Figure 14a,c. Compounds with lignin presented better fits, but considerable discrepancy is still observed for some cooling rates. PBAT/PLA/lignin 90 KGy showed maximum discrepancy of −19% for 5°C/min, more prominent in the nucleation and primary crystallization phase, for other rates the maximum discrepancy was −9%. PBAT/PLA/lignin with 30 and 60 KGy showed intermediate discrepancies. Indicating that for the investigated materials Vyazovkin model is more representative in *Ea* evaluation.

The rigorous determination of crystallization kinetics parameters presented in this work can help in the adequate selection of processing conditions at different temperatures, for instance, the time and temperature necessary to reach a defined relative crystallinity, which is directly linked to polymer properties. Furthermore, predictions are among the most important practical features of kinetic analysis. They are widely used to assess the kinetic behavior of materials beyond the temperature regions of experimental measurements. For example, thermal stability can be estimated as the time to reach a specific degree of conversion at certain temperature. These kinetic predictions can be easily performed using *Ea* dependence evaluated by an isoconversional method, such as Friedman and Vyazovkin methods discussed in this work.

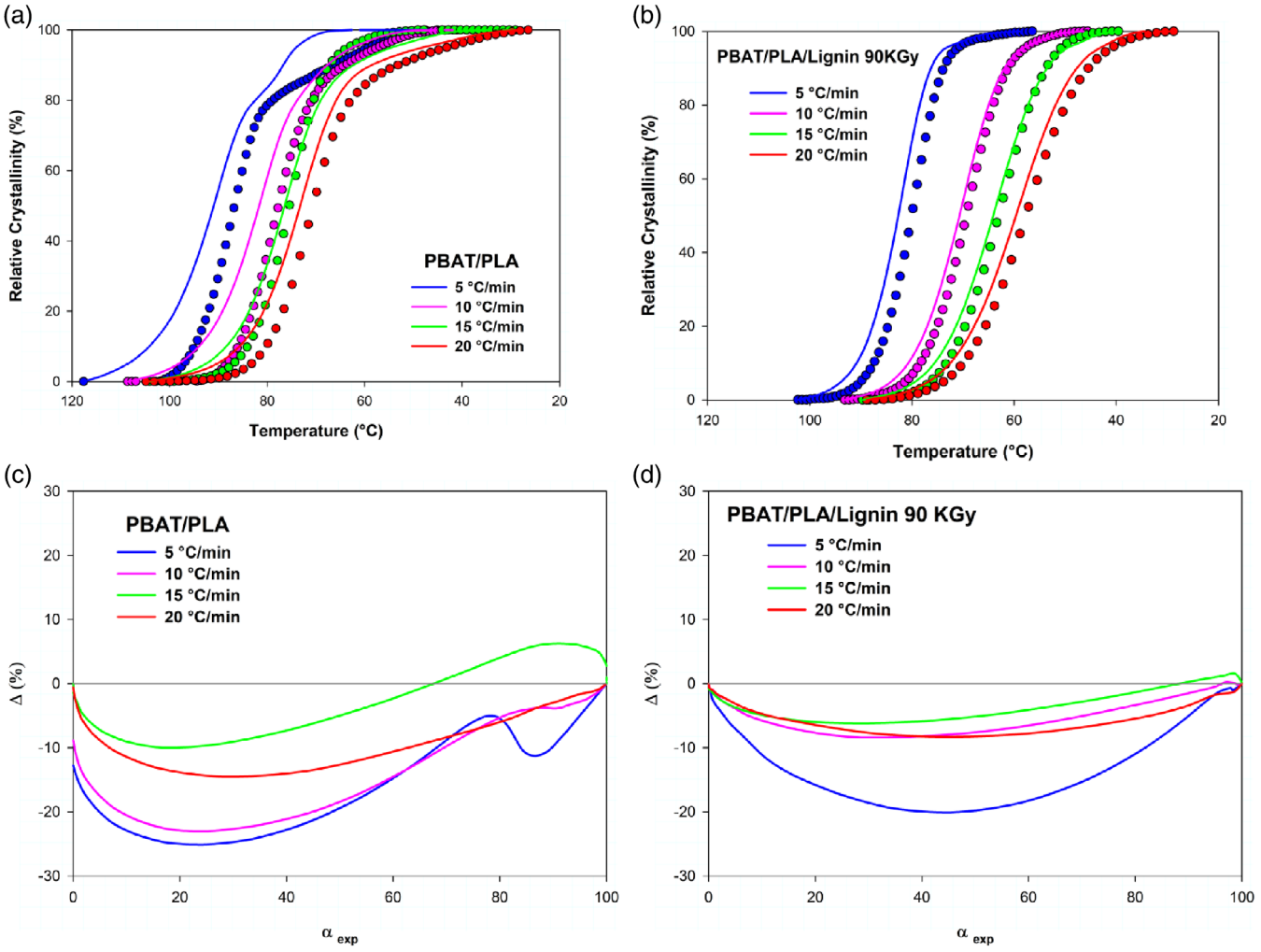

FIGURE 14 (a) and (b) Relative crystallinity as temperature function, experimental (symbols) and theoretical (solid line) data evaluated using Vyazovkin model. (c) and (d) Discrepancy between experimental and theoretical data (Δ) using Vyazovkin model at indicated heating rates and blends. [Color figure can be viewed at wileyonlinelibrary.com]

3.7 | Field emission scanning electron microscopy (FESEM)

The cryogenic fracture surfaces of PBAT/PLA and investigated PBAT/PLA/lignin non-irradiated and irradiated compounds are shown in Figure 15.

In Figure 15a, it can be verified that PBAT/PLA presents biphasic morphology typical of immiscible systems, with PLA spheroidal domains dispersed in PBAT matrix. This is due to the reduced interaction and different surface tension between PBAT and PLA.[58]

Upon non-irradiated lignin addition, it is observed that the lignin exhibits irregular particles embedded in the PBAT/PLA matrix. Some lignin particles were pulled-out from the matrix surface; this implies gaps in wettability between PBAT/PLA and lignin and/or weakness in interfacial adhesion. It can be seen that lignin particles were projected out of the surface, indicating that there was low compatibility between PBAT/PLA and non-irradiated lignin.[59,60]

PBAT/PLA/lignin irradiated at absorbed doses of 30, 60, and 90 KGy, unlike PBAT/PLA and the PBAT/PLA/lignin, showed an improved interface between polymers, that is, there was less phase segregation between PBAT and PLA, indicating that lignin irradiation affects the blend compatibility, corroborating FTIR data, where the intermolecular interactions between the PBAT/PLA carbonyl and the lignin hydroxyl groups were verified, corroborating miscibility between components. In addition, there was decrease in pull-out lignin particles, it is also observed that lignin is more adhered and covered by the PBAT/PLA blend, presenting more homogeneous aspect without evident voids and gaps, indicating better dispersion and interaction. Similar results were obtained for PBAT/PLA/$CaCO_3$, where it was observed greater compatibility of PBAT/PLA upon addition of $CaCO_3$[61]

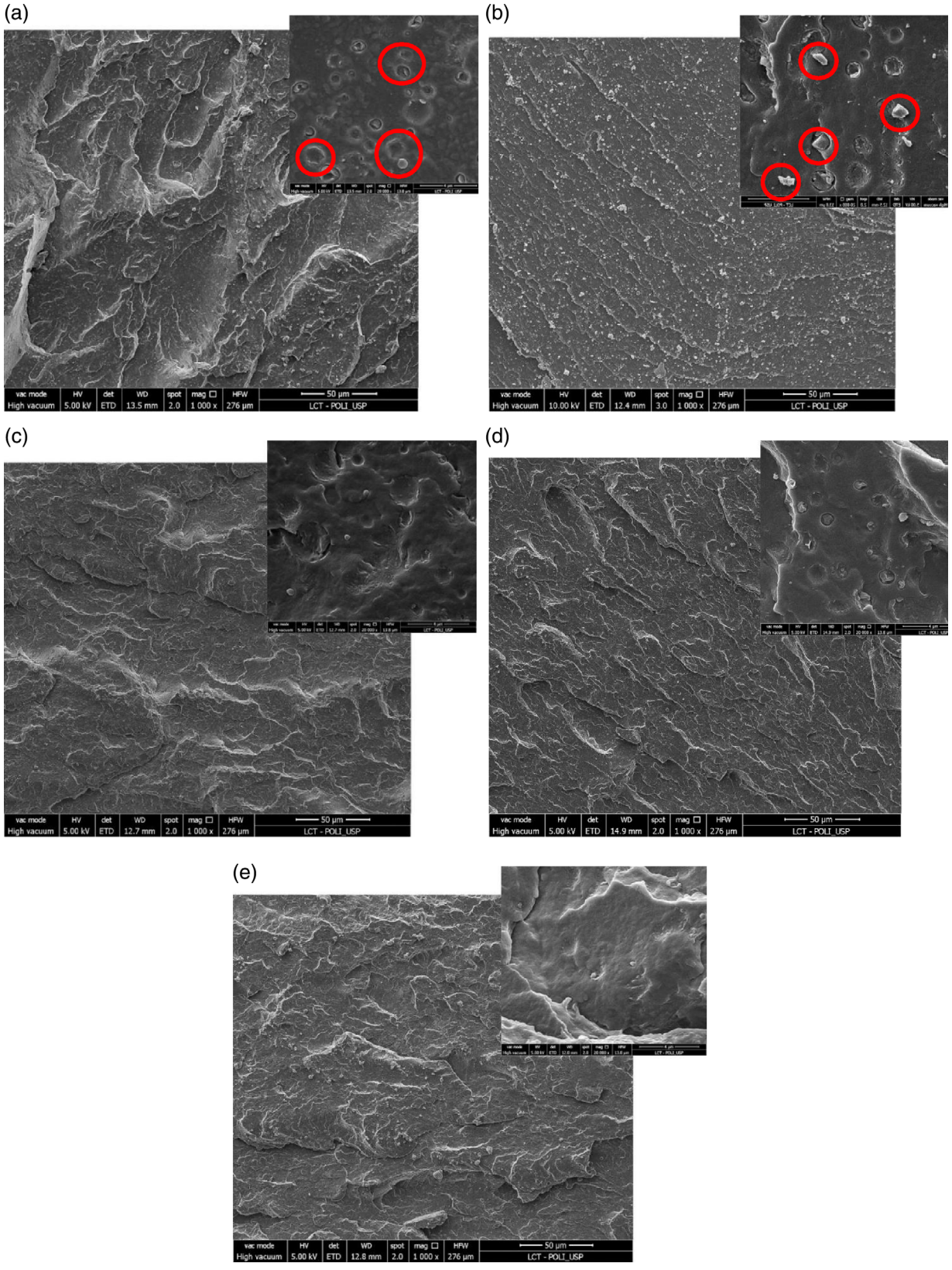

FIGURE 15 FE-SEM images of fracture surfaces (a) PBAT/PLA, (b) PBAT/PLA/lignin, (c) PBAT/PLA/lignin 30 KGy, (d) PBAT/PLA/lignin 60 KGy, (e) PBAT/PLA/lignin 90 KGy. Voltage (5.000 kV) and magnification (1.000× and 20.000×). FE-SEM, Field emission scanning electron microscopy; PBAT, Poly(butylene adipate-co-terephthalate); PLA, Poly(lactic acid) [Color figure can be viewed at wileyonlinelibrary.com]

Regarding the fracture, there is a change in the fracture surface trend upon lignin addition. In Figure 15a greater plastic deformation is observed where parts of fractured material are projected upwards and with rough regions, since with lignin addition, the morphology underwent changes, especially the non-irradiated lignin, where the surface presents regions more planes and the crack propagation occur in a more continuous way, characteristic of brittle fracture. Upon addition of irradiated lignin, the surfaces more closely resemble the PBAT/PLA surface.

The data report that addition of irradiated lignin in PBAT/PLA is very promising. Gamma radiation improved compatibility, as observed by FTIR spectra and DSC scans, also corroborated by SEM images, as well as an improved interfacial adhesion between PBAT/PLA/lignin was verified. Therefore, having great potential to be used in thermoplastic applications with differentiated properties, particularly for the segments of biodegradable food packaging materials and agricultural mulching films.

4 | CONCLUSION

PBAT/PLA/lignin blends based on non-irradiated and irradiated lignin were successfully produced. Gamma irradiation provided significant changes in lignin chemical structure, as observed in FTIR spectra, such as improved miscibility and compatibility, resulted from secondary interaction between PBAT/PLA carbonyl and lignin hydroxyls, directly influencing the thermal properties of lignin and blends, such as decrease in temperature and crystallization rate. The non-isothermal crystallization kinetics using Pseudo-Avrami, Friedman, and Vyazovkin isoconversional modeling was significant, providing energy evaluation along with the whole crystallization. From SEM images of fracture surface of PBAT/PLA/irradiated lignin presented better dispersion and compatibility, having great potential to promote blends improvements. This research elucidates that lignin irradiation can be an effective route for its functionalization and application in polymeric systems, with great potential for thermoplastic applications, especially for the production of biodegradable food packaging materials and mulching films.

AUTHOR CONTRIBUTIONS

Janetty Jany Pereira Barros : Conceptualization (lead); data curation (lead); software (lead); writing – original draft (lead). **Carlos Pereira Soares**: Investigation (supporting). **Esperidiana Augusta Barretos de Moura**: Methodology (lead); resources (lead); supervision (lead); validation (lead); writing – review and editing (lead). **Renate Maria Ramos Wellen**: Data curation (lead); methodology (lead); resources (lead); supervision (lead); validation (lead); writing – review and editing (lead).

FUNDING INFORMATION

The authors would like to thank the financial support from the Fundação de Apoio à Pesquisa do Estado de São Paulo (FAPESP) Process Number 2019/00862-9 (Concession term: June/2019 – Professor Esperidiana A. B. Moura); IAEA-CRP No. 17760/RO (Concession term: September/2013 – Professor Esperidiana A. B. Moura); Coordenação de Aperfeiçoamento de Pessoal de Nível Superior (CAPES), from Conselho Nacional de Desenvolvimento Científico e Tecnológico (CNPq); and Fundação de Apoio à Pesquisa do Estado da Paraíba (FAPESQ) (Concession term: 017/2019). Professor Renate Wellen is CNPq fellow (Number: 303426/2021-7); Janetty Jany Pereira Barros is CAPES fellow (Number: 88887.569630/2020-00).

CONFLICT OF INTEREST

The authors declare no conflicts of interest.

DATA AVAILABILITY STATEMENT

The data that support the findings of this study are available in the supplementary material of this article.

ORCID

Janetty Jany Pereira Barros https://orcid.org/0000-0001-9618-6062

REFERENCES

[1] D. Kun, B. Pukánszky, *Eur. Polym. J.* **2017**, *93*, 618.
[2] J.-L. Wen, S.-L. Sun, B.-L. Xue, R.-C. Sun, *Materials* **2013**, *6*, 359.
[3] W. Gao, P. Fatehi, *Can. J. Chem. Eng.* **2019**, *97*, 2827.
[4] C. Jiang, H. He, H. Jiang, L. Ma, D. Jia, *Express Polym. Lett.* **2013**, 7, 480.
[5] U. P. Perera, M. L. Foo, K. W. Tan, I. M. L. Chew, *IOP Conf. Ser.: Mater. Sci. Eng.* **2019**, *652*, 012054.
[6] M. S. Ferreira, M. N. Sartori, R. R. Oliveira, O. Guven, E. A. Moura, *Appl. Surf. Sci.* **2014**, *310*, 325.
[7] O. Güven, S. N. Monteiro, E. A. Moura, J. W. Drelich, *Polym. Rev.* **2016**, *56*, 702.
[8] P. Criado, C. Fraschini, M. Jamshidian, S. Salmieri, A. Safrany, M. Lacroix, *Cellulose* **2017**, *24*, 2111.
[9] N. Rajeswara Rao, T. Venkatappa Rao, S. Ramana Reddy, B. Sanjeeva Rao, *J. Radiat. Res. Appl. Sci.* **2015**, *8*, 621.
[10] T. Islam, R. A. Khan, M. A. Khan, M. A. Rahman, M. Fernandez-Lahore, Q. Huque, R. Islam, *Polym.-Plast. Technol. Eng.* **2009**, *48*, 1198.
[11] M. M. El-Zayat, A. Abdel-Hakim, M. A. Mohamed, *J. Macromol. Sci. A.* **2019**, *56*, 127.
[12] R. Mehta, V. Kumar, H. Bhunia, S. Upadhyay, *J. Macromol. Sci. Polymer Rev.* **2005**, *45*, 325.

[13] L.-T. Lim, R. Auras, M. Rubino, *Prog. Polym. Sci.* **2008**, *33*, 820.
[14] L. C. Arruda, M. Magaton, R. E. S. Bretas, M. M. Ueki, *Polym. Test.* **2015**, *43*, 27.
[15] M. Evstatiev, S. Simeonova, K. Friedrich, X.-Q. Pei, P. Formanek, *J. Mater. Sci.* **2013**, *48*, 6312.
[16] A. Kumar, V. R. Tumu, S. R. Chowdhury, R. R. SVS, *Int. J. Biol. Macromol.* **2019**, *121*, 588.
[17] R. Chen, M. A. Abdelwahab, M. Misra, A. K. Mohanty, *J. Polym. Environ.* **2014**, *22*, 439.
[18] Y. Ding, B. Lu, P. Wang, G. Wang, J. Ji, *Polym. Degrad. Stab.* **2018**, *147*, 41.
[19] S. Qiu, Y. Zhou, G. I. Waterhouse, R. Gong, J. Xie, K. Zhang, J. Xu, *Food Chem.* **2021**, *334*, 127487.
[20] R. M. Patel, J. E. Spruiell, *Polym. Eng. Sci.* **1991**, *31*, 730.
[21] M. H. Boutaous, N. Brahmia, P. Bourgin, *Comptes Rendus Mecanique* **2010**, *338*, 78.
[22] Y. Wang, C. Shen, H. Li, Q. Li, J. Chen, *J. Appl. Polym. Sci.* **2004**, *91*, 308.
[23] J. J. P. Barros, I. D. dos Santos Silva, N. G. Jaques, R. M. R. Wellen, *J. Mater. Res. Technol.* **2020**, *9*, 13539.
[24] S. Girdthep, W. Limwanich, W. Punyodom, *Mater. Chem. Phys.* **2022**, *276*, 125227.
[25] N. Shi, Q. Dou, *J. Therm. Anal. Calorim.* **2015**, *119*, 635.
[26] W. Phetwarotai, D. Aht-Ong, *J. Therm. Anal. Calorim.* **2016**, *126*, 1797.
[27] S. A. Arruda, J. C. D. Sousa, J. C. Lima, M. D. B. C. Vitorino, E. L. Canedo, Y. M. B. D. Almeida, *Mater. Res.* **2018**, *21, 0213*.
[28] S. Vyazovkin, D. Dollimore, *J. Chem. Inf. Comput. Sci.* **1996**, *36*, 42.
[29] K. Dimitra, C. Konstantinos, *Thermochim. Acta* **2021**, *704*, 179030.
[30] S. Vyazovkin, N. Sbirrazzuoli, *Macromol. Rapid Commun.* **2006**, *27*, 1515.
[31] M. Avrami, *J. Chem. Phys.* **1939**, *7*, 1103.
[32] M. Avrami, *J. Chem. Phys.* **1941**, *9*, 177.
[33] S. V. C. R. Coutinho, A. B. de Sousa Barros, J. J. P. Barros, A. K. C. Albuquerque, J. V. M. Barreto, D. D. Siqueira, A. Ries, R. M. R. Wellen, *J. Appl. Polym. Sci.* **2021**, *138*, 50807.
[34] A. Ries, E. L. Canedo, C. R. Souto, R. M. Wellen, *Thermochim. Acta* **2016**, *637*, 74.
[35] R. M. Wellen, E. L. Canedo, *J. Mater. Res.* **2016**, *31*, 729.
[36] H. L. Friedman, *J. Polym. Sci., Part C: Polym. Symp.* **1964**, 183, 183.
[37] G. Antoniadis, K. Paraskevopoulos, A. Vassiliou, G. Papageorgiou, D. Bikiaris, K. Chrissafis, *Thermochim. Acta* **2011**, *521*, 161.
[38] R. Svoboda, J. Málek, *Thermochim. Acta* **2011**, *526*, 237.
[39] N. Rajeswara Rao, T. Venkatappa Rao, S. Ramana Reddy, B. Sanjeeva Rao, *Advanced Mater. Lett.* **2015**, *6*, 560.
[40] Y.-F. Cheng, Q. Shen, *Int. Wood Prod. J.* **2018**, *9*, 186.
[41] X. Wu, L. Chen, J. Chen, X. Su, Y. Liu, K. Wang, W. Qin, H. Qi, M. Deng, *Waste Biomass Valoriz.* **2019**, *10*, 3025.
[42] A. Ayoub, R. A. Venditti, H. Jameel, H. M. Chang, *J. Appl. Polym. Sci.* **2014**, *131*, 131.
[43] M. Wojdyr, *J. Appl. Crystallogr.* **2010**, *43*, 1126.
[44] X. Wang, Y. Jia, Z. Liu, J. Miao, *Polymer* **2018**, *10*, 1013.
[45] B. M. Carvalho, M. C. G. Pellá, J. C. Hardt, A. R. de Souza Rossin, A. Tonet, T. Ilipronti, J. Caetano, D. C. Dragunski, *J. Mol. Liq.* **2021**, *325*, 115206.
[46] L.-F. Wang, J.-W. Rhim, S.-I. Hong, *LWT–Food Sci. Technol.* **2016**, *68*, 454.
[47] D. P. Facchi, P. R. Souza, V. C. Almeida, E. G. Bonafé, A. F. Martins, *J. Mol. Liq.* **2021**, *321*, 114476.
[48] C. Wang, S. S. Kelley, R. A. Venditti, *ChemSusChem* **2016**, *9*, 770.
[49] L. Jiang, M. P. Wolcott, J. Zhang, *Biomacromolecules* **2006**, *7*, 199.
[50] S. Livi, V. Bugatti, M. Marechal, B. G. Soares, G. M. Barra, J. Duchet-Rumeau, J.-F. Gérard, *RSC Adv.* **2015**, 5, 1989.
[51] J. W. Huang, *J. Polym. Sci., Part B: Polym. Phys.* **2008**, *46*, 564.
[52] Q. Xing, D. Ruch, P. Dubois, L. Wu, W.-J. Wang, *ACS Sustainable Chem. Eng.* **2017**, *5*, 10342.
[53] D. D. Siqueira, C. B. Luna, E. M. Araújo, A. B. Barros, R. M. R. Wellen, *Polym. Adv. Technol.* **2021**, *32*, 3572.
[54] F. M. Sousa, A. R. M. Costa, L. T. Reul, F. B. Cavalcanti, L. H. Carvalho, T. G. Almeida, E. L. Canedo, *Polym. Bull.* **2019**, *76*, 1573.
[55] P. Das, P. Tiwari, *Thermochim. Acta* **2017**, *654*, 191.
[56] S. Vyazovkin, *Phys. Chem. Chem. Phys.* **2016**, *18*, 18643.
[57] S. Vyazovkin, N. Sbirrazzuoli, *J. Therm. Anal. Calorim.* **2003**, *72*, 681.
[58] S. Vyazovkin, *Int. J. Chem. Kinet.* **1996**, *28*, 95.
[59] M. A. Anwer, H. E. Naguib, A. Celzard, V. Fierro, *Composites, Part B* **2015**, *82*, 92.
[60] J. Guo, X. Chen, J. Wang, Y. He, H. Xie, Q. Zheng, *Polymer* **2019**, *12*, 56.
[61] D. B. Rocha, J. Souza de Carvalho, S. A. de Oliveira, D. dos Santos Rosa, *J. Appl. Polym. Sci.* **2018**, *135*, 46660.

SUPPORTING INFORMATION

Additional supporting information can be found online in the Supporting Information section at the end of this article.

How to cite this article: J. J. P. Barros, C. P. Soares, E. A. B. de Moura, R. M. R. Wellen, *J. Appl. Polym. Sci.* **2022**, *139*(45), e53124. https://doi.org/10.1002/app.53124